JIB-04 has broad-spectrum antiviral activity and inhibits SARS-CoV-2 replication and coronavirus pathogenesis

Juhee Son[1,2,*], Shimeng Huang[3,*], Qiru Zeng[1,*], Traci L. Bricker[4], James Brett Case[4], Jinzhu Zhou[3], Ruochen Zang[1,5], Zhuoming Liu[1], Xinjian Chang[3], Houda H. Harastani[4], Lu Chen[6], Maria Florencia Gomez Castro[1], Yongxiang Zhao[3], Hinissan P. Kohio[1], Gaopeng Hou[1], Baochao Fan[3], Beibei Niu[3], Rongli Guo[3], Paul W. Rothlauf[1,7], Adam L. Bailey[8], Xin Wang[5], Pei-Yong Shi[9], Elisabeth D. Martinez[10], Sean P.J. Whelan[1], Michael S. Diamond[1,4,8], Adrianus C.M. Boon[1,4,8], Bin Li[3,#], Siyuan Ding[1,#]

[1]Department of Molecular Microbiology, Washington University School of Medicine, St. Louis, MO, USA. [2]Program in Molecular Cell Biology, Washington University School of Medicine, St. Louis, MO, USA. [3]Institute of Veterinary Medicine, Jiangsu Academy of Agricultural Sciences, Nanjing, China. [4]Department of Medicine, Division of Infectious Diseases, Washington University School of Medicine, St. Louis, MO, USA. [5]Key Laboratory of Marine Drugs, Ministry of Education, Ocean University of China, Qingdao, China. [6]National Center for Advancing Translational Sciences, National Institutes of Health, Rockville, MD, USA. [7]Program in Virology, Harvard Medical School, Boston, MA, USA. [8]Department of Pathology and Immunology, Washington University School of Medicine, St. Louis, MO, USA. [9]Department of Biochemistry and Molecular Biology, University of Texas Medical Branch, Galveston TX, USA. [10]Department of Pharmacology, UT Southwestern Medical Center, Dallas, TX 75390, USA.

* These authors contributed equally: Juhee Son, Shimeng Huang, Qiru Zeng

Corresponding authors: Bin Li, libinana@126.com, Siyuan Ding, siyuan.ding@wustl.edu

Abstract

Pathogenic coronaviruses represent a major threat to global public health. Here, using a recombinant reporter virus-based compound screening approach, we identified several small-molecule inhibitors that potently block the replication of the newly emerged severe acute respiratory syndrome virus 2 (SARS-CoV-2). Among them, JIB-04 inhibited SARS-CoV-2 replication in Vero E6 cells with an EC_{50} of 695 nM, with a specificity index of greater than 1,000. JIB-04 showed *in vitro* antiviral activity in multiple cell types against several DNA and RNA viruses, including porcine coronavirus transmissible gastroenteritis virus. In an *in vivo* porcine model of coronavirus infection, administration of JIB-04 reduced virus infection and associated tissue pathology, which resulted in improved weight gain and survival. These results highlight the potential utility of JIB-04 as an antiviral agent against SARS-CoV-2 and other viral pathogens.

INTRODUCTION

The coronavirus disease 2019 (COVID-19) pandemic has caused unprecedented global morbidity, mortality, and socioeconomic destabilization. Thus, there is an urgent unmet need to develop safe and effective countermeasures to combat the disease beyond vaccine protection and provide immediate treatment. Multiple efforts are underway to

identify candidate drugs that inhibit the replication of severe acute respiratory syndrome virus 2 (SARS-CoV-2) (Riva *et al.*, 2020; Touret *et al.*, 2020; Dittmar *et al.*, 2021; Heiser *et al.*, 2020; Mirabelli *et al.*, 2020), the cause of COVID-19 (Wu *et al.*, 2020; Zhou *et al.*, 2020). So far, several small-molecule inhibitors that interfere with SARS-CoV-2 cell entry have been identified, including transmembrane serine protease inhibitors camostat (Hoffmann *et al.*, 2020) and nafamostat (Wang *et al.*, 2020a), and endosomal inhibitors including chloroquine and its derivatives (Wang *et al.*, 2020a), E-64d (Hoffmann *et al.*, 2020), apilimod (Kang *et al.*, 2020), and 25-hydroxycholesterol (Zang *et al.*, 2020a). Drug screens and structural studies also revealed compounds that target the viral enzymes of SARS-CoV-2, namely the RNA-dependent RNA polymerase (Yin *et al.*, 2020; Gao *et al.*, 2020; Kirchdoerfer and Ward, 2019; Nguyen *et al.*, 2020; Sheahan *et al.*, 2020) and the main protease (M^{pro}, also known as $3CL^{pro}$) (Zhang *et al.*, 2020; Dai *et al.*, 2020; Jin *et al.*, 2020; Nguyen *et al.*, 2020). Here, utilizing a fluorescent SARS-CoV-2 virus and an imaging-based screen approach, we identified several known and previously unknown antiviral compounds that inhibit SARS-CoV-2 replication.

RESULTS

To identify small molecules with anti-SARS-CoV-2 activity, we performed a screen using a recombinant SARS-CoV-2 that encoded mNeonGreen as a reporter of infection (Xie *et al.*, 2020) and an in-house collection of ~200 compounds that comprised FDA-approved drugs, well-defined broad-spectrum antiviral agents, and investigational new drugs. We identified 157 compounds that had greater antiviral efficacy (>44.8% inhibition) than either

70 chloroquine or remdesivir against SARS-CoV-2 replication in Vero E6 cells (**Fig. 1A** and
71 **Dataset S1**). One of these drugs was a pan-Jumonji histone demethylase inhibitor 5-
72 chloro-N-[(E)-[phenyl(pyridin-2-yl)methylidene]amino]pyridin-2-amine (JIB-04 E-isomer)
73 (Wang *et al.*, 2013) (**Fig. S1A**). We selected JIB-04 (JIB-04 E-isomer, unless noted
74 otherwise) for further characterization because several histone demethylases were
75 recently discovered as SARS-CoV-2 host dependency factors (Wei *et al.*, 2021; Wang *et*
76 *al.*, 2021; Schneider *et al.*, 2021) and JIB-04 has not been reported as an antiviral
77 molecule, despite its established anti-tumor activity (Wang *et al.*, 2013; Kim *et al.*, 2018;
78 Parrish *et al.*, 2018; Bayo *et al.*, 2018; Dalvi *et al.*, 2017).
79
80 We tested whether JIB-04 treatment could inhibit replication of a clinical isolate of SARS-
81 CoV-2 (2019-nCoV/USA-WA1/2020 strain). Viral antigen staining showed that a 1-hour
82 pre-treatment with JIB-04 suppressed SARS-CoV-2 infection in Vero E6 cells with an
83 EC_{50} value of 695 nM (95% confidence interval of 567-822 nM) (**Fig. 1B**). Cell viability did
84 not fall below 50% even at 1 mM of JIB-04 treatment, making the selectivity index of JIB-
85 04 higher than 1,000. Intracellular SARS-CoV-2 RNA levels also were reduced
86 significantly by JIB-04, but not by camostat, a TMPRSS serine protease inhibitor (**Fig.**
87 **1C**).
88
89 To examine whether JIB-04 targets SARS-CoV-2 spike protein-mediated entry or other
90 post-entry pathways (*e.g.*, translation, replication, or assembly) shared between SARS-
91 CoV-2 and other viruses, we tested JIB-04 against vesicular stomatitis virus (VSV) that
92 expresses eGFP as a marker of infection (Cherry *et al.*, 2005) and a replication-

93 competent chimeric VSV in which the native glycoprotein (G) was replaced by the spike
94 of SARS-CoV-2 (VSV-eGFP-SARS-CoV-2) (Case *et al.*, 2020). JIB-04 suppressed
95 replication of both viruses in MA104 and Vero E6-TMPRSS2 cells (**Fig. 2A-B**). Flow
96 cytometry analysis of cells at 6h post-infection revealed a reduction in eGFP expression
97 demonstrating that the inhibitory effect of JIB-04 occurs during either entry or gene-
98 expression (**Fig. 2B**). Virus-infected cells also showed less GFP intensity with JIB-04
99 treatment (**Fig. S2A**). JIB-04 inhibited VSV-SARS-CoV-2 infection dose-dependently
100 without apparent cytotoxicity (**Fig. 2C** and **S2B**), which became more apparent when cells
101 were inoculated with virus at a low multiplicity of infection (MOI) (**Fig. S2C**). At 30 μM,
102 JIB-04 treatment resulted in a 100-fold reduction of intracellular VSV-SARS-CoV-2 RNA
103 levels (**Fig. S2D**).
104
105 We next evaluated the antiviral activity of JIB-04 against other viruses. Though JIB-04 did
106 not diminish replication of herpes simplex virus 1, it inhibited the replication of vaccinia
107 virus, another DNA virus, and several strains of rotavirus (RV), a double-stranded RNA
108 virus (RV) (**Fig. 2C-D**). JIB-04 also inhibited the replication of transmissible gastroenteritis
109 virus (TGEV) (**Fig. 2D-E** and **Fig. S2E**), a porcine coronavirus that infects the small
110 intestine of pigs and causes lethal diarrhea (Saif, 2004). This indicates that the antiviral
111 effect of JIB-04 is not limited to single-stranded RNA viruses in cell culture.
112
113 Although JIB-04 inhibits the replication of both SARS-CoV-2 and VSV-SARS-CoV-2 in
114 monkey kidney epithelial cell lines, a primary *in vivo* target of SARS-CoV-2 is ciliated
115 airway epithelial cells (Hou *et al.*, 2020). We therefore examined the inhibitory effect if

116 JIB-04 on SARS-CoV-2 infection of the human lung epithelial cell line Calu-3 (Hoffmann
117 *et al.*, 2020; Sheahan *et al.*, 2020). We validated that JIB-04 retained its antiviral activity
118 against VSV-SARS-CoV-2 in Calu-3 cells (**Fig. 2G**). VSV-SARS-CoV-2 replication was
119 also inhibited by JIB-04 in HEK293 cells ectopically expressing human ACE2, an entry
120 receptor for SARS-CoV-2 (Hoffmann *et al.*, 2020), with or without ectopic TMPRSS2
121 expression (**Fig. 2G**).
122
123 We next sought to understand the mechanisms of antiviral activity of JIB-04. Although
124 JIB-04 has been previously connected to interferon (IFN) and autophagy activation (Wang
125 *et al.*, 2013; Xu *et al.*, 2018), the antiviral activity that we observed was independent of
126 these pathways. JIB-04 treatment did not lead to the induction of IFN and IFN-stimulated
127 gene expression or the formation of LC3-positive punctate structures (**Fig. S3A-B**). To
128 explore the mechanisms of antiviral action, we utilized a drug combination approach.
129 When a combination of JIB-04 with chloroquine was evaluated based on the highest
130 single agent (HAS) synergy model with SynergyFinder 2.0 (Ianevski *et al.*, 2020), JIB-04
131 was shown to exert a synergistic antiviral effect with chloroquine in MA104 cells (**Fig. 3A**).
132 A combination of JIB-04 and camostat also was synergistically antiviral in Calu-3 cells
133 (**Fig. S3C**), indicating that JIB-04 likely targets a different pathway.
134
135 A possible antiviral role for JIB-04 at a post-entry step was supported by the time of
136 addition experiments (**Fig. 3B**). A 1-h pre-treatment of cells with JIB-04 reduced SARS-
137 CoV-2 spike mRNA transcription following VSV-SARS-CoV-2 infection (**Fig. 3C**), and
138 translation of newly synthesized spike protein, which could not be achieved with

139 Actinomycin D treatment (**Fig. 3D**). These results suggest that JIB-04 might repress virus
140 replication by interfering with the viral RNA transcription or stability.
141
142 We also assessed whether the antiviral activity of JIB-04 is linked to its epigenetic
143 modulatory action. Unlike its E-isomer, the Z-isomer of JIB-04 does not inhibit histone
144 demethylases at similar doses (Wang *et al.*, 2013). When we compared the antiviral
145 efficacy of these two JIB-04 isomers against VSV-SARS-CoV-2 in MA104 cells, the Z-
146 isomer did not inhibit the replication of virus (**Fig. 3E)**. The disparity between the isomers
147 suggests that epigenetic enzyme inhibition is involved in antiviral mechanisms of JIB-04.
148 To examine the cellular pathways modulated by JIB-04, we performed small interfering
149 RNA (siRNA)-mediated knockdown of JIB-04 cellular targets (*i.e.*, histone demethylases
150 KDM4B, KDM4C, KDM5A, or KDM5B (Wang *et al.*, 2013)). Knockdown of each gene
151 successfully recapitulated the antiviral effect of JIB-04 (**Fig. 3F** and **Fig. S3E**). These
152 results led us to hypothesize that JIB-04 treatment promoted H3K9 and H3K27
153 methylation and silenced expression of a subset of genes, triggering the antiviral effect.
154 To identify potential target genes, we performed RNA-sequencing on the cells pre-treated
155 with vehicle or JIB-04 with or without virus infection (**Fig. 3G**). Pathway analysis revealed
156 dampened metabolic signaling pathways such as cytochrome P450 system in JIB-04
157 treated cells (**Fig. S3F**). Specifically, JIB-04 treatment downregulated two cytochrome
158 P450 enzymes, *CYP1A1* and *CYP1B1*, and aryl hydrocarbon receptor repressor (*AHRR*),
159 which represses transactivator of *CYP1A1* and *CYP1B1* (Karchner *et al.*, 2002). We
160 validated by quantitative PCR that JIB-04 treatment reduced *CYP1A1*, *CYP1B1*, and
161 *AHRR* mRNA levels by 4-6-fold (**Fig. 3H**). To explore the pharmacological utility of this

162 finding, we tested the antiviral activity of cytochrome P450 enzyme inhibitors fluoxetine
163 and fluvoxamine (Hemeryck and Belpaire, 2002). Both compounds inhibited the
164 replication of VSV-SARS-CoV-2 (**Fig. 3I**) and wild-type SARS-CoV-2 (**Fig. 3J**).
165
166 Given that JIB-04 prevents coronavirus replication *in vitro*, we used a neonatal pig TGEV
167 infection model (Luo *et al.*, 2019) to assess the efficacy of JIB-04 against coronavirus
168 infection *in vivo*. Two-day old piglets were injected via an intraperitoneal route with JIB-
169 04 twice before the oral inoculation of TGEV (**Fig. 4A**). We monitored body weight on a
170 daily basis and recorded diarrhea development and mortality every 6 h. The animals in
171 the control group lost more weight and had more severe diarrhea than those receiving
172 JIB-04 (**Fig. S4A-B**). At 2 days post infection, 3 of 5 piglets in the DMSO group
173 succumbed to infection as compared to 1 out of 5 animals in the JIB-04 group (**Fig. 4B**).
174 Consistent with our *in vitro* results (**Fig. 2E-F**), the TGEV viral burden throughout the
175 gastrointestinal tract was substantially lower in the JIB-04 treated group (**Fig. 4C-D**). JIB-
176 treated animals also had lower number of viral antigen positive cells in their intestinal
177 epithelium (**Fig. S4C**) and showed less enteropathy than the control group (**Fig. 4E**).
178 Taken together, our data demonstrate *in vivo* antiviral activity of JIB-04 against a porcine
179 coronavirus.
180
181 **DISCUSSION**
182
183 Using a repurposed compound screening approach, we identified drugs with reported
184 inhibitory activity against SARS-CoV-2, such as tetrandrine (Ou *et al.*, 2020) and arbidol

185 (Wang *et al.*, 2020b). We also characterized a number of small-molecules (JIB-04, AG-
186 1478, nigericin, etc.) without known antiviral activity as inhibitors of SARS-CoV-2 infection.
187 While this manuscript was in preparation, a new study identified thapsigargin, the
188 compound that showed the highest anti-SARS-CoV-2 activity in our screen as a broad
189 antiviral against coronavirus (Al-Beltagi *et al.*, 2021), which validates our screen approach.
190 Notably, several top hit compounds in the screen converge on the endosomal trafficking
191 pathway: brefeldin A, concanamycin A, tetrandrine, and U18666A. Furthermore, FTY720
192 induced formation of enlarged endosome/lysosome structure, similar to that triggered by
193 apilimod treatment (Kang *et al.*, 2020). All of these point to an important role of endosomal
194 trafficking in SARS-CoV-2 entry and infection, at least in cell culture.
195
196 Our results highlight JIB-04 as a potential therapeutic for SARS-CoV-2 and suggest
197 further evaluation of this drug that has mainly been associated with its anti-cancer
198 activities. Another compound in our screen, GSK-J4, also is a histone demethylase
199 inhibitor that targets KDM6B. However, unlike JIB-04, GSK-J4 failed to reduce viral
200 burden in Vero E6 cells upon SARS-CoV-2 infection to an extent comparable to
201 chloroquine. Thus, we speculate that there might be specific roles played by certain KDM
202 family members in the interactions between the host and SARS-CoV-2.
203
204 **Limitations of the study**
205
206 We have tried to be careful about establishing the broad-spectrum antiviral activity of JIB-
207 04. Indeed, we have shown examples from distinct virus families (double-strand DNA

208 virus: vaccinia virus; single-strand positive-strand RNA virus: SARS-CoV-2 and TGEV;
209 single-strand negative-strand RNA virus: VSV and VSV-SARS-CoV-2; double-strand
210 RNA virus: rotavirus). However, we have yet to test single-strand DNA viruses and
211 retroviruses. We also did not examine whether JIB-04 has antiviral activity against the
212 newly emerging SARS-CoV-2 variants. We showed that JIB-04 modulates cytochrome
213 P450 genes and targeting these genes by well-established selective serotonin uptake
214 inhibitor also led to the inhibition of SARS-CoV-2 replication. Nevertheless, we do not
215 know how modulation of cytochrome P450 genes correlates with transcriptional
216 repression of SARS-CoV-2 RNA that we observed after JIB-04 treatment. It is plausible
217 that JIB-04 induces these two effects separately, which needs to be characterized in
218 future studies. Lastly, though we provided evidence that JIB-04 protects against
219 coronavirus infection *in vivo* using a porcine TGEV model, TGEV is an animal coronavirus
220 that targets the enteric rather than the respiratory system. Protection against SARS-CoV-
221 2 *in vivo* should be tested in a transgenic mouse or hamster model. Finally, while the
222 distinct efficacy of the E vs Z isomers points to inhibition of Jumonji demethylases as
223 contributing to the antiviral effects, direct evidence of this mechanism in multiple models
224 would strengthen this conclusion.
225

226 **MATERIALS AND METHODS**

227 **Reagents, cells, and viruses**

228 **Reagents:** JIB-04 E-isomer used in *in vitro* assays (S7281, Selleckchem, 99.8% purity),
229 JIB-04 E-isomer used in *in vivo* experiments (HY-13953, Med-ChemExpress),
230 Actinomycin D (A5156, Sigma), Fluvoxamine maleate (S1336, Selleckchem), Fluoxetine

231 HCl (S1333, Selleckchem), low molecular weight poly(I:C) complexed with LyoVec (tlrl-
232 picwlv, InvivoGen). EGFP-LC3 plasmid was a gift from Christina Stallings at Washington
233 University School of Medicine. pUC19 empty plasmid was used as mock in all transfection
234 experiments. JIB-04 Z-isomer used in control experiments by synthesized as originally
235 described (Wang et al, 2013).
236
237 **Cells:** Vero E6 cells (CRL-1586, ATCC) and Vero cells (CCL81, ATCC) were cultured in
238 DMEM supplemented with 10% fetal bovine serum (FBS), 10 mM HEPES, 1 mM sodium
239 pyruvate, 0.1 mM non-essential amino acids, and 1X Penicillin-Streptomycin-Glutamine.
240 Calu-3 cells (HTB-55, ATCC) and swine ST cells (CRL-1746, ATCC) were DMEM
241 supplemented with 10% FBS and 1 X Penicillin-Streptomycin-Glutamine. HEK293,
242 HEK293-hACE2, and HEK293-hACE2-TMPRSS2 cells were cultured in complete DMEM
243 containing G418 and/or blasticidin and used as previously described (Zang *et al.*, 2020a).
244 MA104 and Vero E6-TMPRSS2 cells were cultured as before (Zang *et al.*, 2020b).
245
246 **Viruses:** Rhesus RV RRV strain, bovine RV UK strain, and porcine RV NJ2012 strain
247 (Genbank: MT874983-MT874993) were propagated and titrated as before (Ding *et al.*,
248 2018). Vaccinia virus MVA strain was used as before (Li *et al.*, 2017). HSV-1 syn17+
249 strain was a gift from Ann Arvin at Stanford University. TGEV JS2012 strain was
250 propagated as before (Guo *et al.*, 2020). TGEV was titrated by serial dilutions in cells in
251 96-well plates that were seeded at a density of 1 X 10^4 cells per well. Cytopathic effects
252 were observed at 3-7 dpi and the $TCID_{50}$ values were calculated and converted to PFU/ml.
253 A clinical isolate of SARS-CoV-2 (2019-nCoV/USA-WA1/2020 strain) was obtained from

254 the Centers for Disease Control and Prevention. A SARS-CoV-2 mNeonGreen reporter
255 virus was used as previously reported (Xie *et al.*, 2020). Both the clinical isolate and the
256 mNeonGreen SARS-CoV-2 viruses were propagated in Vero CCL81 cells and titrated by
257 focus-forming assays on Vero E6 cells. Recombinant VSV-eGFP (Cherry *et al.*, 2005)
258 and VSV-eGFP-SARS-CoV-2 were previously described (Case *et al.*, 2020). Cells
259 infected with viruses expressing GFP were imaged with an ECHO REVOLVE 4
260 fluorescence microscope. Plaque assays were performed in MA104 cells seeded in 6-
261 well plates using an adapted version of the rotavirus plaque assay protocol (Ding *et al.*,
262 2018).
263
264 **Inhibitor screen**
265 The small-molecule inhibitors used in this study are from in-house collection and the
266 COVID Box (Medicines for Malaria Venture; www.mmv.org/mmv-open/covid-box).
267 Compound names, vendors, and catalog numbers are listed in **Table S1**. At 24 hpi, cells
268 were fixed in 4% paraformaldehyde (PFA) in PBS and stained with Hoechst 33342. The
269 levels of viral antigens, reflected by mNeonGreen signals, were scanned by Amersham
270 Typhoon 5 (GE). Image background was subtracted using rolling ball algorithm (radius =
271 5 pixels). To minimize imaging artifacts and well-to-well variation, we removed the region
272 which fell below the threshold calculated by Moments algorithm. The number of positive
273 pixels and total intensity (after background subtraction) were computed for each well and
274 log10 transformed. The number of cells in each well was quantified based on Hoechst
275 33342 staining detected by Cytation 3 imaging reader (BioTek). Image analysis was

276 performed using ImageJ and customized R scripts. The quantification of mNeonGreen
277 and Hoechst 33342 is provided in **Dataset S1**.
278
279 **Cell cytotoxicity assay**
280 The viability of Vero E6 and MA104 cells after drug treatment was determined using the
281 Cell Counting Kit 8 (ab228554, Abcam). Briefly, cells in 96-well plates were treated with
282 JIB-04 at desired concentrations at 37°C. After a 25-h incubation, the inhibitor-containing
283 medium was replaced with fresh complete medium with 10 µl of WST-8 solution in each
284 well. The cells were incubated at 37 °C for 2 h with protection from light. Absorbance at
285 460nm was measured using Gen5 software and a BioTek ELx800 Microplate Reader.
286
287 **RNA extraction and quantitative PCR**
288 Total RNA was extracted from cells using RNeasy Mini kit (Qiagen). For spike plasmid
289 transfection experiments, total RNA was extracted using Aurum Total RNA Mini Kit
290 (Biorad) with DNase digestion. Complementary DNA was synthesized with High Capacity
291 cDNA Reverse Transcription kit (Thermo Fisher) as previously described (Bolen *et al.*,
292 2013). Quantitative PCR was performed using AriaMX (Agilent) with 12.5 µl of either
293 Power SYBR Green master mix or Taqman master mix (Applied Biosystems) in a 25 µl
294 reaction. Gene expression was normalized to the housekeeping gene GAPDH. All SYBR
295 Green primers and Taqman probes used in this study are listed in **Table S2**.
296
297 **Western blotting**

298 Cells were lysed in RIPA buffer supplemented with protease inhibitor cocktail and
299 phosphatase inhibitor. Lysates were boiled for 5 min in 1 x Laemmli Sample Buffer (Bio-
300 Rad) containing 5% β-mercaptoethanol. Proteins were resolved in SDS-PAGE and
301 detected as described(Ding *et al.*, 2014) using the following antibodies: GAPDH (631402,
302 Biolegend), rotavirus VP6 (rabbit polyclonal, ABclonal technology), and SARS-CoV-2 S2
303 (40592-T62, Sino Biological). Secondary antibodies were anti-rabbit (7074, Cell Signaling)
304 or anti-mouse (7076, Cell Signaling) immunoglobulin G horseradish peroxidase-linked
305 antibodies. Protein bands were visualized with Clarity ECL Substrate (Bio-rad) and a
306 Biorad Gel Doc XR system.
307
308 **Small interfering RNA transfection**
309 HEK293 cells were transfected using Lipofectamine RNAiMAX Transfection Reagent
310 (Thermo Fisher). Cells were harvested at 48 h post transfection, and knockdown
311 efficiency was determined by RT-qPCR. siRNA transfected cells were infected with PoRV
312 (MOI=0.01) for 12 h and viral RNA copy numbers were examined by RT-qPCR. All siRNA
313 used in this study were designed and synthesized by GenePharma (Shanghai, China)
314 and their sequences of siRNAs are listed in **Table S2**.
315
316 **Flow cytometry**
317 Vero E6-TMPRSS2 cells were inoculated with VSV-GFP or VSV-SARS-CoV-2 at an MOI
318 of 3 for 1 h at 37°C. At 6 hpi, cells were harvested and fixed in 4% PFA in PBS. Percentage
319 of GFP positive cells and GFP intensity were determined by BD LSRFortessa™ X-20 cell
320 analyzer and analyzed by FlowJo v10.6.2 (BD).

321

322 **RNA-sequencing**

323 HEK293 cells were pre-treated with JIB-04 (10 μM) for 12 h, and mock or porcine RV-
324 infected (MOI=0.01) for another 12 h. Total RNA from cells in triplicate was extracted
325 using RNeasy Mini kit (Qiagen). RNA sample quality was measured by both NanoDrop
326 spectrophotometer (Thermo Fisher) and Bioanalyzer 2100 (Agilent). Libraries were
327 sequenced on the Illumina NovaSeq 6000 platform. Differential gene expression analysis
328 was performed using DESeq2. The RNA-seq raw and processed datasets were deposited
329 onto NCBI Gene Expression Omnibus database (GSE156219).

330

331 **TGEV piglet infection**

332 Newborn piglets (Landrace × Yorkshire) were spontaneously delivered from sows, and
333 their body weights were recorded at birth. Fifteen neonatal male pigs at birth were
334 obtained from a TGEV-free farm in Nanjing without suckling. All piglets were confirmed
335 negative for TGEV by RT-PCR and ELISA (IDEXX, USA). The pigs were randomly
336 separated into three groups, housed in separate rooms, and fed the same artificial milk
337 substitutes that meet the nutrient and energy recommendations of the National Research
338 Council [NRC, 2012] at the animal facility of the Institute of Veterinary Medicine, Jiangsu
339 Academy of Agricultural Sciences, Nanjing, Jiangsu Province. The experiments were
340 divided into three groups: a DMSO inoculation control group (control, n=5); a DMSO
341 inoculation and TGEV infection group (TGEV-DMSO, n=5); a JIB-04 inoculation and
342 TGEV infection group (TGEV-JIB-04, n=5)). Neonatal pigs were intraperitoneally injected
343 twice with JIB-04 (75 mg/kg) or DMSO at 24 h and 6 h prior to TGEV infection. TGEV-

344 DMSO and TGEV-JIB-04 groups were orally infected with $1\times10^{7.25}$ (1.778×10^{7}) $TCID_{50}$
345 (equivalent to 1.245×10^{7} PFU) of TGEV in 1.5 ml of DMEM per pig. Neonatal pigs were
346 weighed and observed for clinical signs every 8 h throughout the study. Serum samples
347 were collected from each pig at 24 and 48 hpi to detect specific anti-TGEV antibodies.
348 The occurrence of diarrhea was monitored, and its severity was recorded based on an
349 established scoring system (Li *et al.*, 2017). In brief, diarrhea was scored on the basis of
350 color, consistency, and amount, and numbered as follows: 0 = normal; 1 = pasty; 2 =
351 semi-liquid; 3 = liquid, and score ≥ 2 considered as diarrhea. At 48 hpi, all pigs were
352 euthanized, and intestinal tissues were collected for pathological examination and viral
353 load analysis using RT-qPCR and primers in **Table S2**.
354

355 **Histopathological and immunofluorescence analysis**

356 Intestinal tissues harvested from pigs were fixed in 4% PFA in PBS and incubated in 50%
357 ethanol overnight. After fixation, tissues were embedded in paraffin, sectioned, and
358 subjected to hematoxylin and eosin staining by standard procedures. For
359 immunofluorescence analysis, samples were incubated with rabbit anti-TGEV-N antibody
360 (1:500, DA0224, Shanghai YouLong Biotech) for 30 min at 37 ºC. After three washes,
361 samples were stained with Cy3-conjugated goat anti-rabbit secondary antibody
362 (Beyotime) and DAPI (Invitrogen). Images were obtained using a fluorescence
363 microscope (Carl Zeiss).
364

365 **Ethics statement**

366 Animal experiments were approved by the Committee on the Ethics of Animal Care and
367 Use of the Science and Technology Agency of Jiangsu Province. The approval ID is
368 NKYVET 2014-63, granted by the Jiangsu Academy of Agricultural Sciences
369 Experimental Animal Ethics Committee. All efforts were made to minimize animal
370 suffering. The virus challenge and tissue collection were performed in strict accordance
371 with the guidelines of Jiangsu Province Animal Regulations (Decree No. 2020-18).
372

373 **Statistical analysis**

374 All bar graphs were displayed as means ± standard error of mean (SEM). Statistical
375 significance in data Fig. 2E, 2F, 3C, 4C, and 4D was calculated by Student's *t* test using
376 Prism 8.4.3 (GraphPad). Statistical significance in data Fig. 1C, 2D, 2G, 3B, 3E, 3G, S3A,
377 S3C, and S4B was calculated by pairwise ANOVA using Prism 8.4.3. Non-linear
378 regression (curve fit) was performed to calculate EC_{50} and CC_{50} values for Fig. 1B, 2A,
379 and 2C using Prism 8.4.3. HSA synergy model was used to calculate the synergy scores
380 of dose-response data in Fig. 3A. Gehan-Breslow-Wilcoxon test was used to compare
381 the survival curves in Fig. 4B. All data were presented as asterisks (*$p \leq 0.05$; **$p \leq 0.01$;
382 ***$p \leq 0.001$). All experiments other than Fig. 1A, 3I, and 4 were repeated at least twice.
383 The raw data are included in **Table S3**.
384

385 **SUPPLEMENTARY MATERIALS**

386 Table S1. List of chemicals used in the anti-SARS-CoV-2 compound screen
387 Table S2. List of qPCR primers and siRNA
388 Table S3. Raw data
389

390 **Figures and Legends**

391

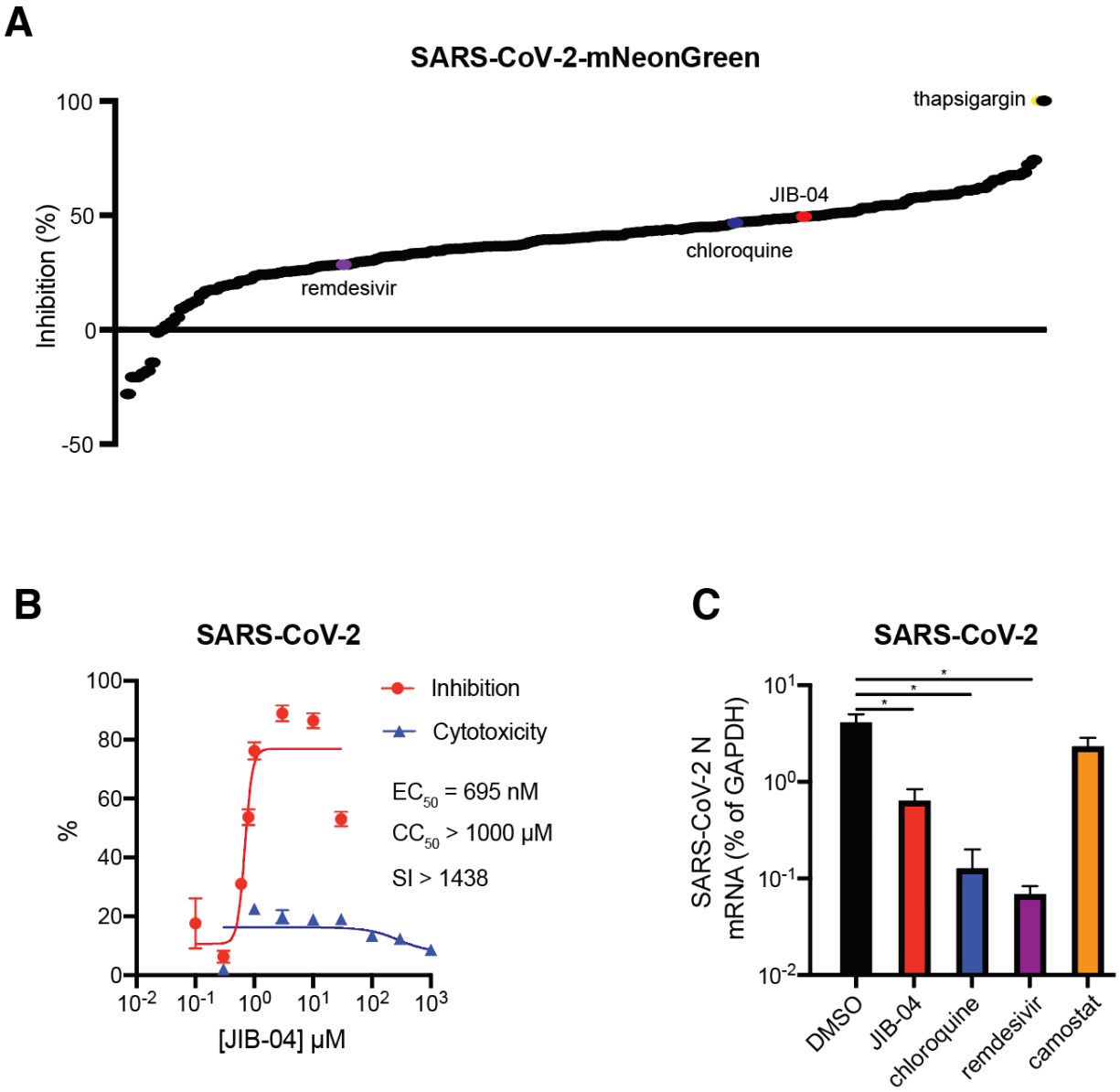

392

393

394 **Fig. 1. JIB-04 inhibits SARS-CoV-2 replication**

395 (A) Small molecule inhibitor screen. Vero E6 cells were treated with individual

396 compounds (listed in Table S1) at 10 μM for 1 hour (h) and infected with SARS-

397 CoV-2-mNeonGreen (MOI=0.5). At 24 h post infection (hpi), cells were fixed, and

398 nuclei were stained by Hoechst 33342. The intensities of mNeonGreen and

399 Hoechst were quantified by the Typhoon biomolecular imager and the Cytation
400 plate reader, respectively. The ratio of mNeonGreen and Hoechst is plotted as
401 percentage of inhibition.
402 (B) Dose-response curve of wild-type SARS-CoV-2 replication with JIB-04 treatment.
403 Vero E6 cells were treated with JIB-04 for 1 h and infected with a clinical isolate of
404 SARS-CoV-2 (MOI=0.5). S protein levels were quantified at 24 hpi based on
405 immunofluorescence. For CC_{50} measurement, cells were treated with JIB-04 at 0.3
406 μM to 1 mM for 25 h. SI: selectivity index.
407 (C) Intracellular viral RNA levels of cells treated with compounds and subsequently
408 infected with wild-type SARS-CoV-2. Vero E6 cells were treated with JIB-04 (10
409 μM), chloroquine (10 μM), remdesivir (3 μM), or camostat (10 μM) for 1 h and
410 infected with a clinical isolate of SARS-CoV-2 (MOI=0.5). SARS-CoV-2 RNA levels
411 at 24 hpi were measured by RT-qPCR.
412 For all panels except A, experiments were repeated at least three times with similar
413 results. Fig. 1A was performed once with raw data included in Dataset S1. Data
414 are represented as mean ± SEM. Statistical significance is from pooled data of the
415 multiple independent experiments (*$p \leq 0.05$).
416

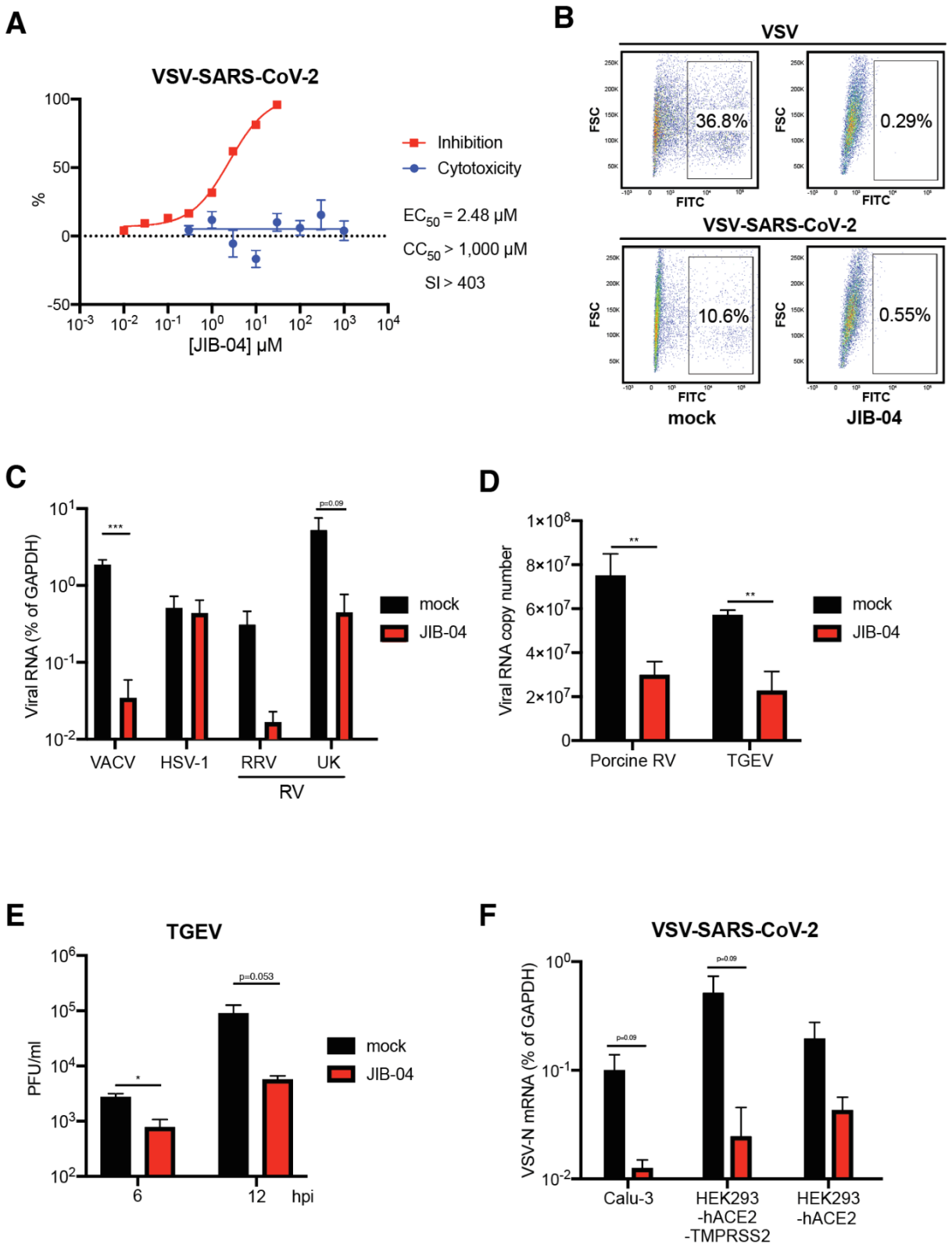
A
VSV-SARS-CoV-2
100
50
0
-50
%
10^{-3} 10^{-2} 10^{-1} 10^{0} 10^{1} 10^{2} 10^{3} 10^{4}
[JIB-04] μM
Inhibition
Cytotoxicity
EC_{50} = 2.48 μM
CC_{50} > 1,000 μM
SI > 403
B
VSV
FSC
FITC
36.8%
0.29%
VSV-SARS-CoV-2
10.6%
0.55%
mock
JIB-04
C
Viral RNA (% of GAPDH)
10^{1}
10^{0}
10^{-1}
10^{-2}
***
p=0.09
VACV
HSV-1
RRV
UK
RV
mock
JIB-04
D
Viral RNA copy number
1×10^{8}
8×10^{7}
6×10^{7}
4×10^{7}
2×10^{7}
0
**
**
Porcine RV
TGEV
mock
JIB-04
E
TGEV
PFU/ml
10^{6}
10^{5}
10^{4}
10^{3}
10^{2}
*
p=0.053
6
12
hpi
mock
JIB-04
F
VSV-SARS-CoV-2
VSV-N mRNA (% of GAPDH)
10^{0}
10^{-1}
10^{-2}
p=0.09
p=0.09
Calu-3
HEK293
-hACE2
-TMPRSS2
HEK293
-hACE2

417
418

419 **Fig. 2. JIB-04 broadly inhibits DNA and RNA viruses in different cell types**

420 (A) Dose-response analysis of VSV-SARS-CoV-2 replication and cytotoxicity with JIB-
421 04 treatment. For EC_{50} measurement, MA104 cells were treated with compounds
422 at 0.01 to 30 μM for 1 h and infected with VSV-SARS-CoV-2 (MOI=3) for 24 h. For
423 CC_{50} measurement, cells were treated with compounds at 0.1 μM to 3 mM for 25
424 h. SI: selectivity index.

425 (B) Virus infectivity with JIB-04 treatment. Vero E6-TMPRSS2 cells were treated with
426 compounds (10 μM) for 1 h and infected with VSV or VSV-SARS-CoV-2 (MOI=3).
427 At 6 hpi, percentages of GFP positive cells were quantified by flow cytometry.

428 (C) Intracellular viral RNA levels with JIB-04 treatment. MA104 cells were treated with
429 compounds (10 μM) for 1 h and infected with vaccinia virus (VACV), herpes
430 simplex virus-1 (HSV-1), or rotavirus (RV, RRV and UK strains) (MOI=1). Viral
431 RNA levels at 24 hpi were measured by RT-qPCR for VACV B10R, HSV-1 ICP-
432 27, and RV NSP5, respectively.

433 (D) Viral RNA copy numbers with JIB-04 treatment. HEK293 cells were treated with
434 JIB-04 (10 μM) for 6 h and infected with porcine rotavirus (MOI=0.01) for 6 h. ST
435 cells were treated with JIB-04 (10 μM) for 12 h and infected with transmissible
436 gastroenteritis virus (TGEV) (MOI=0.01) for 12 h. Viral RNA copy numbers were
437 measured by RT-qPCR.

438 (E) TGEV titers in the cell supernatant with JIB-04 treatment. ST cells were treated
439 with JIB-04 (10 μM) for 12 h and infected with TGEV (MOI=0.01). Virus titers at 6
440 and 12 hpi were measured by plaque assays.

441 (F) Intracellular viral RNA levels with JIB-04 treatment in different cell types. Calu-3
442 cells, HEK293-hACE2 and HEK293-hACE2-TMPRSS2 were treated with
443 compounds (10 μM) for 1 h and infected with VSV-SARS-CoV-2 (MOI=1). VSV
444 RNA levels at 24 hpi were measured by RT-qPCR.
445 All experiments were repeated at least three times with similar results. Data are
446 represented as mean ± SEM. Statistical significance is from pooled data of the
447 multiple independent experiments (*$p \leq 0.05$; **$p \leq 0.01$; ***$p \leq 0.001$).
448

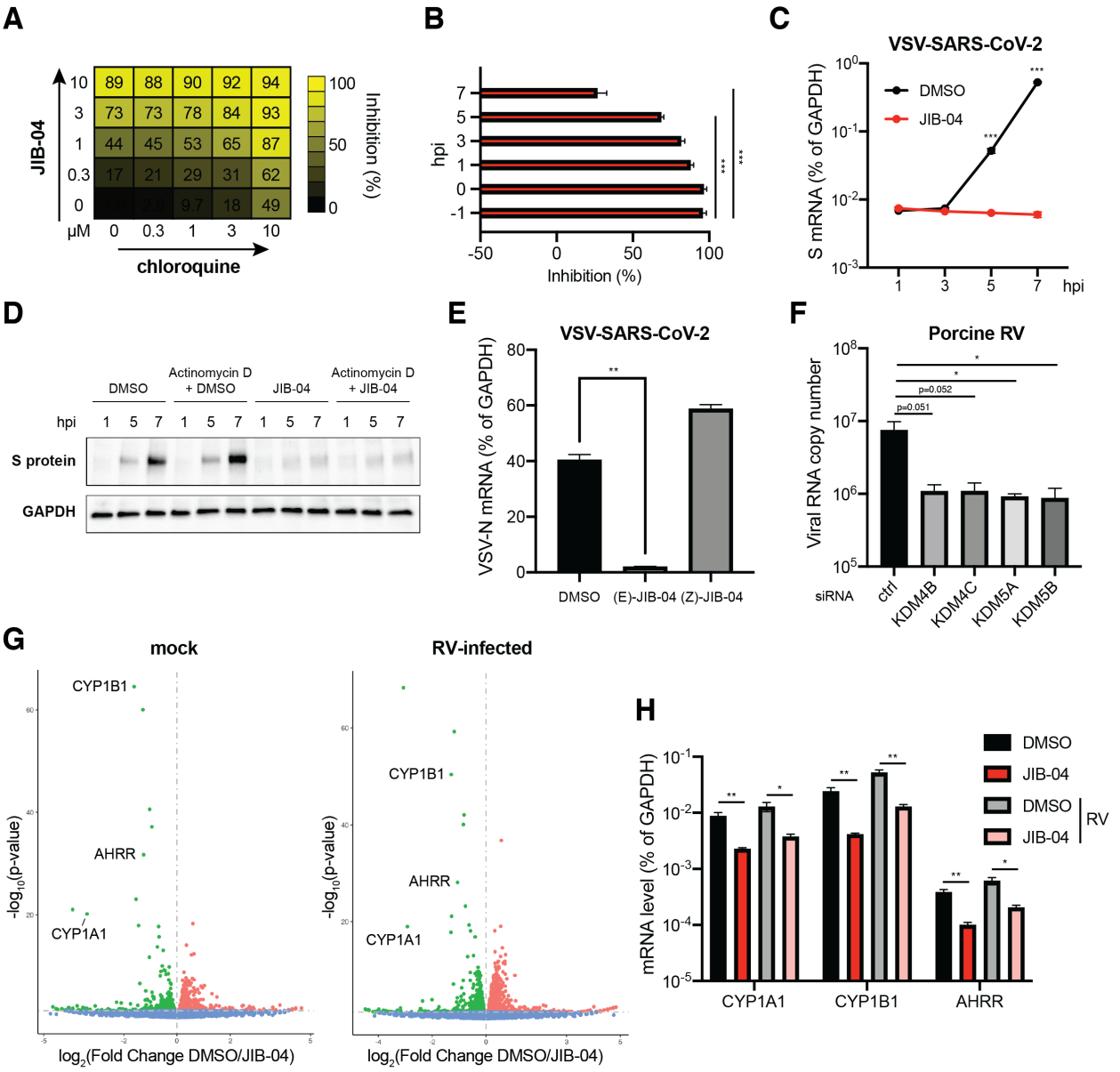
A
JIB-04
10 89 88 90 92 94
3 73 73 78 84 93
1 44 45 53 65 87
0.3 17 21 29 31 62
0 9.7 18 49
μM 0 0.3 1 3 10
chloroquine
100
50
0
Inhibition (%)
B
hpi
7
5
3
1
0
-1
-50 0 50 100
Inhibition (%)
C
VSV-SARS-CoV-2
DMSO
JIB-04
S mRNA (% of GAPDH)
1 3 5 7 hpi
D
DMSO
Actinomycin D + DMSO
JIB-04
Actinomycin D + JIB-04
hpi 1 5 7 1 5 7 1 5 7 1 5 7
S protein
GAPDH
E
VSV-SARS-CoV-2
VSV-N mRNA (% of GAPDH)
DMSO (E)-JIB-04 (Z)-JIB-04
F
Porcine RV
Viral RNA copy number
p=0.051
p=0.052
siRNA ctrl KDM4B KDM4C KDM5A KDM5B
G
mock
RV-infected
CYP1B1
AHRR
CYP1A1
-log10(p-value)
log2(Fold Change DMSO/JIB-04)
H
DMSO
JIB-04
DMSO
JIB-04
RV
mRNA level (% of GAPDH)
CYP1A1 CYP1B1 AHRR
I
VSV-SARS-CoV-2
Inhibition
Cytotoxicity
%
[Fluoxetine] μM
[Fluvoxamine] μM
J
SARS-CoV-2
Inhibition
Cytotoxicity
%
[Fluoxetine] μM
[Fluvoxamine] μM

451 **Fig. 3. JIB-04 exhibits distinct post-entry antiviral mechanisms**

452 (A) Drug combination dose-response matrix and VSV-SARS-CoV-2 replication.
453 MA104 cells were treated with JIB-04 and chloroquine for 1 h and infected with
454 VSV-SARS-CoV-2 (MOI=3). GFP signals at 24 hpi were quantified to calculate the
455 percentage of inhibition.

456 (B) Time of compound addition and VSV-SARS-CoV-2 replication. MA104 cells were
457 treated with JIB-04 (10 μM) at indicated time points relative to VSV-SARS-CoV-2
458 infection (MOI=3, 0 hpi). GFP signals at 8 hpi were quantified to calculate the
459 percentage of inhibition.

460 (C) Intracellular SARS-CoV-2 S RNA levels with JIB-04 treatment. MA104 cells were
461 treated with JIB-04 (10 μM) for 1 h and infected with VSV-SARS-CoV-2 (MOI=1)
462 for 1, 3, 5, and 7 h. S RNA levels were measured by RT-qPCR.

463 (D) Western blot analysis of SARS-CoV-2 S protein levels with JIB-04 treatment.
464 MA104 cells were treated with JIB-04 (10 μM) for 1 h and infected with VSV-SARS-
465 CoV-2 (MOI=1) for 1, 5, and 7 h. For Actinomycin D, 10 μg/ml actinomycin D was
466 added to the media 15 min before DMSO or JIB-04 treatment.

467 (E) Intracellular viral RNA levels of cells treated with JIB-04 E-isomer or Z-isomer and
468 subsequently infected with VSV-SARS-CoV-2. MA104 cells were treated with JIB-
469 04 isomer (10 μM) for 1 h and infected with VSV-SARS-CoV-2 (MOI=1). VSV-N
470 levels at 24 hpi were measured by RT-qPCR.

471 (F) Histone demethylase siRNA knockdown and RV replication. HEK293 cells were
472 transfected with scrambled siRNA or siRNA targeting indicated histone

473 demethylases for 48 h and infected with porcine RV (MOI=0.01). Viral RNA copy
474 numbers at 12 hpi were quantified by RT-qPCR.
475 (G) Volcano plot of differentially expressed transcripts with JIB-04 treatment and RV
476 infection. HEK293 cells were treated with DMSO or JIB-04 (10 μM) for 12 h, and
477 mock-infected (left panel) or infected with porcine RV (MOI=0.01, right panel) for
478 another 12 h. Red dots represent upregulated genes and green dots represent
479 downregulated genes in JIB-04 treated cells.
480 (H) Expression of three top genes in (G) with JIB-04 treatment. HEK293 cells were
481 treated with JIB-04 (10 μM) for 12 h and mock-infected or infected porcine RV
482 (MOI=0.01) for 12 h. mRNA levels of *CYP1A1, CYP1B1, and AHRR* at 12 hpi were
483 measured by RT-qPCR.
484 (I) Dose-response analysis of VSV-SARS-CoV-2 replication with fluoxetine or
485 fluvoxamine treatment. MA104 cells were treated with compounds at 0.01 to 30
486 μM for 1 h and infected with VSV-SARS-CoV-2 (MOI=3). GFP signals at 24 hpi
487 were quantified to calculate the percentage of inhibition. For CC_{50} measurement,
488 cells were treated with compounds at 0.1 μM to 300 μM for 25 h.
489 (J) Dose-response analysis of wild-type SARS-CoV-2 replication with fluoxetine or
490 fluvoxamine treatment. Vero E6 cells were treated with compounds for 1 h and
491 infected with a clinical isolate of SARS-CoV-2 (MOI=0.5). S protein levels at 24 hpi
492 were quantified based on immunofluorescence. For CC_{50} measurement, cells were
493 treated with compounds at 0.1 μM to 300 μM for 25 h.
494 For all panels except A and J, experiments were repeated at least three times with
495 similar results. Fig. 3A was performed twice. Inhibition assay in Fig. 3J was

496 performed once and cytotoxicity assay was performed in triplicates. Data are
497 represented as mean ± SEM. Statistical significance is from pooled data of the
498 multiple independent experiments (*$p \leq 0.05$; **$p \leq 0.01$; ***$p \leq 0.001$).

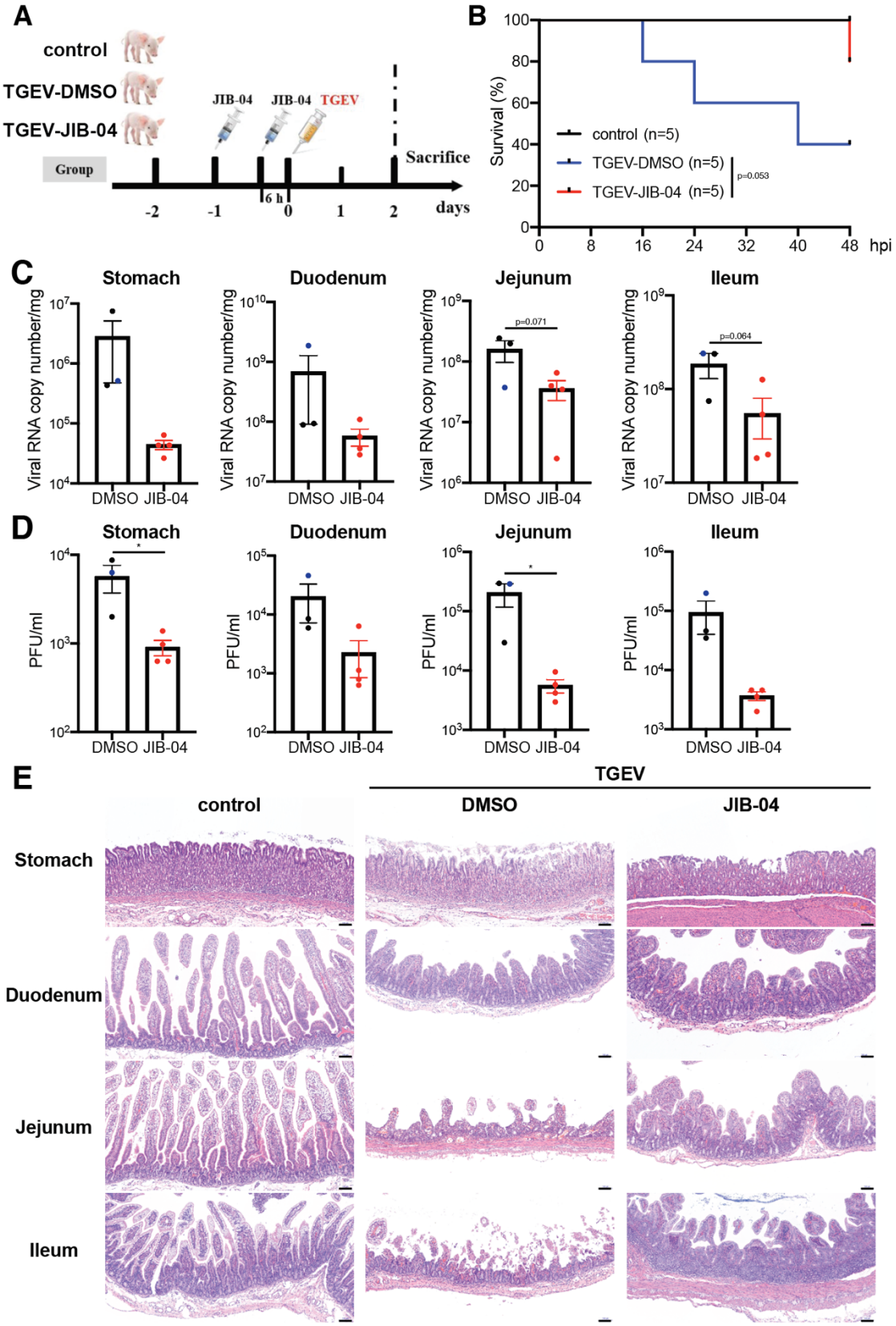
A
control
TGEV-DMSO
TGEV-JIB-04
Group
JIB-04
JIB-04
TGEV
Sacrifice
6 h
-2
-1
0
1
2
days
B
Survival (%)
control (n=5)
TGEV-DMSO (n=5)
TGEV-JIB-04 (n=5)
p=0.053
hpi
C
Stomach
Duodenum
Jejunum
Ileum
Viral RNA copy number/mg
p=0.071
p=0.064
DMSO
JIB-04
D
PFU/ml
E
TGEV
control
DMSO
JIB-04
Stomach
Duodenum
Jejunum
Ileum

501 **Fig. 4. JIB-04 suppresses TGEV replication and pathogenesis in pigs**

502 (A) Experimental schemes for testing the protective efficacy of JIB-04 treatment
503 against TGEV challenge in three groups of neonatal pigs. Control: DMSO injection,
504 mock infection; TGEV-DMSO: DMSO injection, TGEV infection; TGEV-JIB-04:
505 JIB-04 injection, TGEV infection.

506 (B) Survival curve of TGEV infected pigs with JIB-04 treatment. Neonatal pigs were
507 intraperitoneally injected with vehicle control DMSO or JIB-04 and mock-infected
508 or infected with 1.2×10^7 PFU of TGEV. Survival was monitored every 8 h with
509 data censored at 48 hpi, when all pigs were sacrificed.

510 (C) TGEV RNA copy numbers in the gastrointestinal (GI) tract of infected pigs. TGEV
511 infected piglets were sacrificed at 48 hpi. For the DMSO group, two animals
512 sacrificed at 48 hpi and one that died at 40 hpi (colored in blue) were examined.
513 For the JIB-04 groups, four animals sacrificed at 48 hpi were examined. TGEV
514 genome copy numbers at 48 hpi were quantified by RT-qPCR.

515 (D) Same as (C) except that virus titers were measured by plaque assays.

516 (E) Hematoxylin and eosin staining of different GI tract sections from pigs sacrificed at
517 48 hpi. Representative images of 3 animals. Scale bar, 100 μm.

518 Data are represented as mean ± SEM. Statistical significance is from pooled data
519 of the multiple independent experiments (*$p \leq 0.05$).

520

521 **Supplemental Figures and Legends**

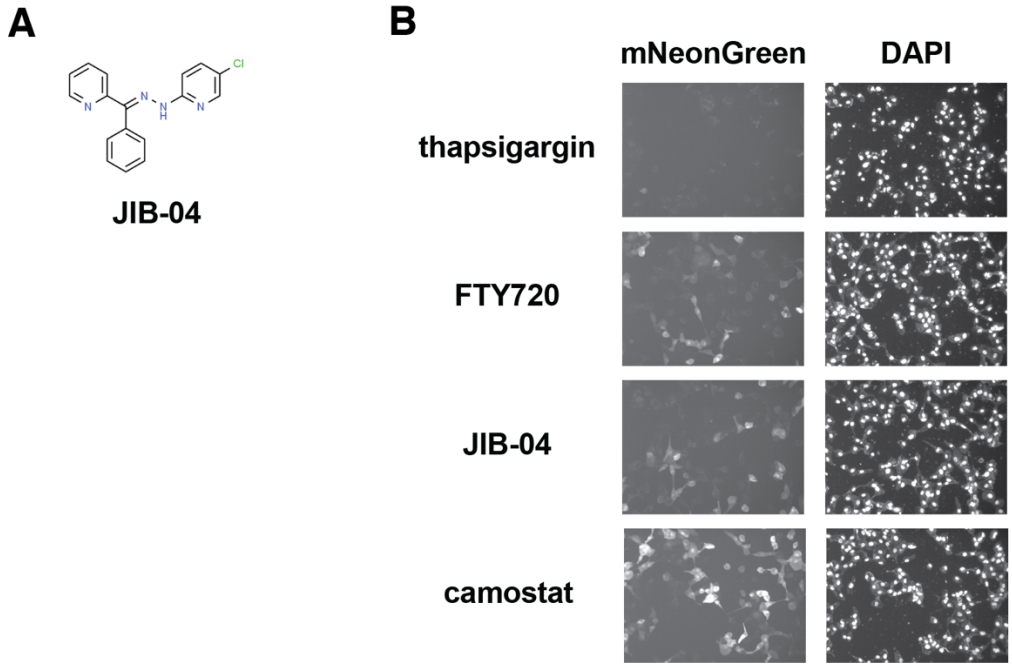

522
523
524 **Fig. S1. JIB-04 inhibits SARS-CoV-2 replication**

525 (A) Chemical structures of JIB-04 E-isomer from ChemSpider database.

526 (B) Representative images of Vero E6 cells infected by SARS-CoV-2-mNeonGreen

527 (MOI=0.5) at 24 hpi in Fig. 1A.

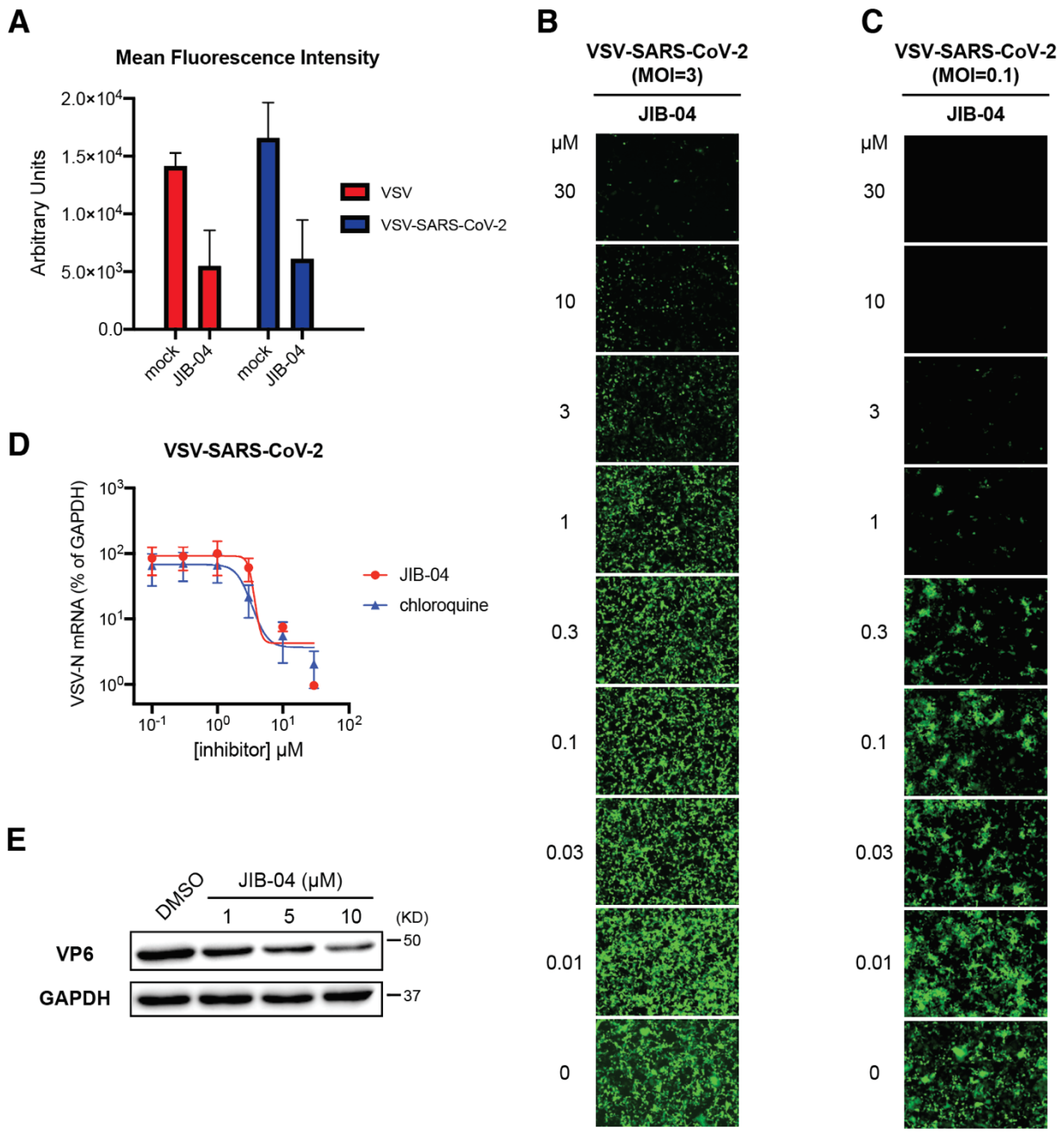

528

529 **Fig. S2. JIB-04 inhibits the replication of multiple viruses**

530 (A) Mean fluorescence intensity of GFP positive cells in Fig. 2B was quantified by flow

531 cytometry.

532 (B) Dose-response analysis of VSV-SARS-CoV-2 replication with JIB-04 treatment.

533 MA104 cells were treated with JIB-04 at indicated concentrations for 1 h and

534 infected with VSV-SARS-CoV-2 (MOI=3). At 24 hpi, images of GFP positive
535 infected cells were acquired by the ECHO fluorescence microscope.
536 (C) Same as (B) except that cells were infected with an MOI of 0.1.
537 (D) Dose-response analysis of intracellular viral RNA levels with JIB-04 or chloroquine
538 treatment. MA104 cells were treated with compounds at 0.1 to 30 μM for 1 h and
539 infected with VSV-SARS-CoV-2 (MOI=3). VSV RNA levels at 24 hpi were
540 measured by RT-qPCR.
541 (E) Western blot analysis of RV antigen VP6 levels with JIB-04 treatment. HEK293
542 cells were treated with JIB-04 at 1, 5, or 10 μM for 6 h and infected with porcine
543 RV (MOI=0.01) for 12 h. GAPDH was used as a loading control.
544 All experiments were repeated at least three times with similar results. Data are
545 represented as mean ± SEM.

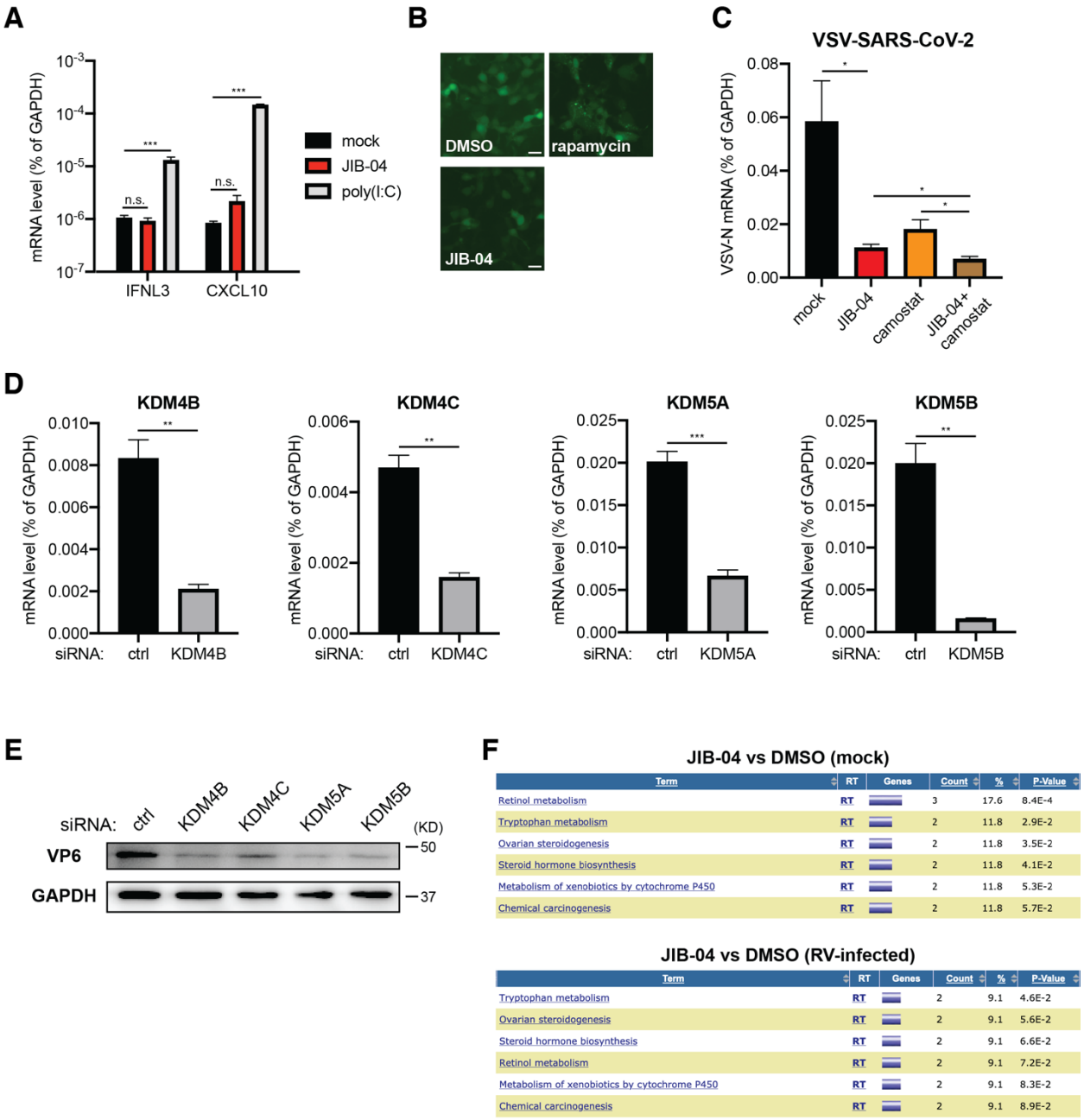

Fig. S3. Inhibition or knockdown of specific KDM histone demethylases inhibits virus replication

(A) Expression of IFN and IFN-stimulated genes with JIB-04 treatment. HEK293 cells were treated with JIB-04 (3 μM) or transfected with low-molecular-weight poly(I:C)

552 (100 ng/ml) for 24 h. mRNA levels of IFNL3 and CXCL10 were measured by RT-
553 qPCR.
554 (B) Autophagy formation with compound treatment. HEK293 cells were transfected
555 with EGFP-LC3 plasmid for 24 h and treated with rapamycin (100 nM) or JIB-04 (3
556 μM) for another 18 h. GFP positive punctate structures indicate autophagy
557 activation. Scale bar, 20 μm.
558 (C) Intracellular viral RNA levels with JIB-04 and camostat treatment. Calu-3 cells were
559 treated with compounds (10 μM) for 1 h and infected with VSV-SARS-CoV-2
560 (MOI=3). VSV RNA levels at 24 hpi were measured by RT-qPCR.
561 (D) siRNA-mediated knockdown of JIB-04 target histone demethylases. HEK293 cells
562 were transfected with scrambled siRNA or siRNA targeting indicated histone
563 demethylases for 48 h. mRNA levels of indicated histone demethylases were
564 measured by RT-qPCR.
565 (E) Western blot analysis of RV antigen VP6 levels in cells with histone demethylase
566 siRNA knockdown. HEK293 cells were transfected with scrambled siRNA or siRNA
567 targeting indicated histone demethylases for 48 h and infected with porcine RV
568 (MOI=0.01) for 12 h.
569 (F) Pathway enrichment analysis of gene expression regulated by JIB-04 treatment.
570 Downregulated genes in Fig. 3F with p values < 1e-10 were analyzed by DAVID
571 functional annotation.
572 For all panels except B, experiments were repeated at least three times with similar
573 results. Fig. S2B was performed twice. Data are represented as mean ± SEM.

574 Statistical significance is from pooled data of the multiple independent experiments

575 (*$p \leq 0.05$; **$p \leq 0.01$; ***$p \leq 0.001$).

576

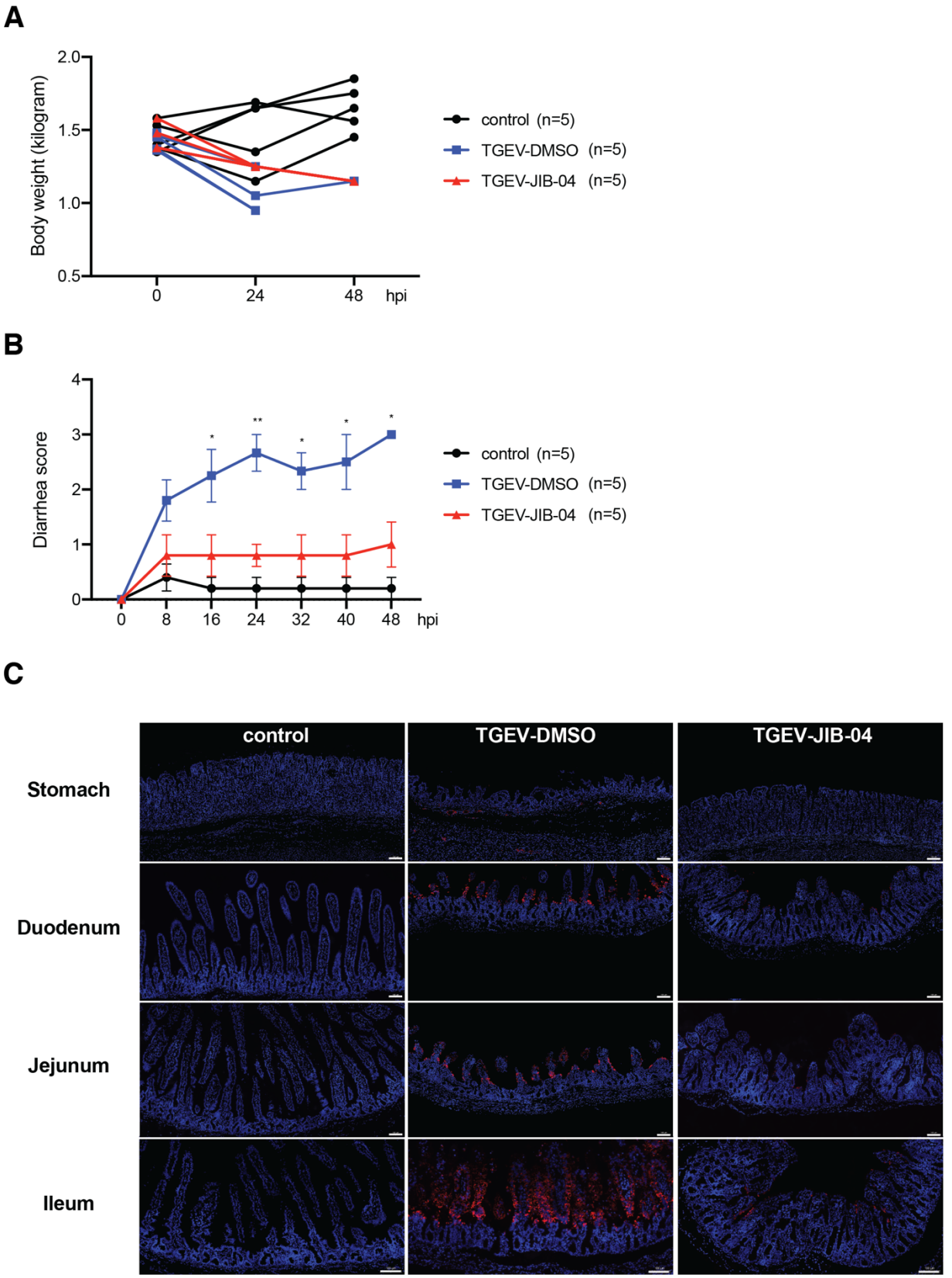
A
Body weight (kilogram)
2.0
1.5
1.0
0.5
0
24
48
hpi
control (n=5)
TGEV-DMSO (n=5)
TGEV-JIB-04 (n=5)
B
Diarrhea score
4
3
2
1
0
0
8
16
24
32
40
48
hpi
control (n=5)
TGEV-DMSO (n=5)
TGEV-JIB-04 (n=5)
C
control
TGEV-DMSO
TGEV-JIB-04
Stomach
Duodenum
Jejunum
Ileum

579 **Fig. S4. JIB-04 reduces TGEV induced weight loss and pathogenesis**

580 (A) Weight of TGEV infected pigs with JIB-04 treatment in Fig. 4B. The body weight of
581 individual animals was monitored every 24 h.

582 (B) Diarrhea occurrence in TGEV infected pigs with JIB-04 treatment in Fig. 4B.
583 Diarrhea severity was scored for the fecal specimens of DMSO or JIB-04 treated,
584 mock or TGEV infected animals every 8 h.

585 (C) Immunofluorescence staining of TGEV antigen in different GI tract sections from
586 pigs sacrificed at 48 hpi. Blue: cell nuclei; red: TGEV nucleocapsid protein.
587 Representative images of 3 animals. Scale bar, 100 μm.

588

589 **REFERENCES**
590
591 Al-Beltagi, S., Preda, C. A., Goulding, L. V., James, J., Pu, J., Skinner, P., Jiang, Z., Wang, B. L., Yang,
592 J., Banyard, A. C., Mellits, K. H., Gershkovich, P., Hayes, C. J., Nguyen-Van-Tam, J., Brown, I. H.,
593 Liu, J. and Chang, K. C. (2021) 'Thapsigargin Is a Broad-Spectrum Inhibitor of Major Human
594 Respiratory Viruses: Coronavirus, Respiratory Syncytial Virus and Influenza A Virus', *Viruses,* 13(2).
595 Bayo, J., Tran, T. A., Wang, L., Pena-Llopis, S., Das, A. K. and Martinez, E. D. (2018) 'Jumonji
596 Inhibitors Overcome Radioresistance in Cancer through Changes in H3K4 Methylation at Double-
597 Strand Breaks', *Cell Rep,* 25(4), pp. 1040-1050 e5.
598 Bolen, C. R., Ding, S., Robek, M. D. and Kleinstein, S. H. (2013) 'Dynamic expression profiling of
599 Type I and Type III Interferon-stimulated hepatocytes reveals a stable hierarchy of gene
600 expression', *Hepatology*.
601 Case, J. B., Rothlauf, P. W., Chen, R. E., Liu, Z., Zhao, H., Kim, A. S., Bloyet, L. M., Zeng, Q., Tahan,
602 S., Droit, L., Ilagan, M. X. G., Tartell, M. A., Amarasinghe, G., Henderson, J. P., Miersch, S., Ustav,
603 M., Sidhu, S., Virgin, H. W., Wang, D., Ding, S., Corti, D., Theel, E. S., Fremont, D. H., Diamond, M.
604 S. and Whelan, S. P. J. (2020) 'Neutralizing Antibody and Soluble ACE2 Inhibition of a Replication-
605 Competent VSV-SARS-CoV-2 and a Clinical Isolate of SARS-CoV-2', *Cell Host Microbe,* 28(3), pp.
606 475-485 e5.
607 Cherry, S., Doukas, T., Armknecht, S., Whelan, S., Wang, H., Sarnow, P. and Perrimon, N. (2005)
608 'Genome-wide RNAi screen reveals a specific sensitivity of IRES-containing RNA viruses to host
609 translation inhibition', *Genes Dev,* 19(4), pp. 445-52.
610 Dai, W., Zhang, B., Su, H., Li, J., Zhao, Y., Xie, X., Jin, Z., Liu, F., Li, C., Li, Y., Bai, F., Wang, H., Cheng,
611 X., Cen, X., Hu, S., Yang, X., Wang, J., Liu, X., Xiao, G., Jiang, H., Rao, Z., Zhang, L. K., Xu, Y., Yang,
612 H. and Liu, H. (2020) 'Structure-based design of antiviral drug candidates targeting the SARS-CoV-
613 2 main protease', *Science*.
614 Dalvi, M. P., Wang, L., Zhong, R., Kollipara, R. K., Park, H., Bayo, J., Yenerall, P., Zhou, Y., Timmons,
615 B. C., Rodriguez-Canales, J., Behrens, C., Mino, B., Villalobos, P., Parra, E. R., Suraokar, M., Pataer,
616 A., Swisher, S. G., Kalhor, N., Bhanu, N. V., Garcia, B. A., Heymach, J. V., Coombes, K., Xie, Y.,
617 Girard, L., Gazdar, A. F., Kittler, R., Wistuba, II, Minna, J. D. and Martinez, E. D. (2017) 'Taxane-
618 Platin-Resistant Lung Cancers Co-develop Hypersensitivity to JumonjiC Demethylase Inhibitors',
619 *Cell Rep,* 19(8), pp. 1669-1684.
620 Ding, S., Khoury-Hanold, W., Iwasaki, A. and Robek, M. D. (2014) 'Epigenetic reprogramming of
621 the type III interferon response potentiates antiviral activity and suppresses tumor growth', *PLoS*
622 *Biol,* 12(1), pp. e1001758.
623 Ding, S., Zhu, S., Ren, L., Feng, N., Song, Y., Ge, X., Li, B., Flavell, R. A. and Greenberg, H. B. (2018)
624 'Rotavirus VP3 targets MAVS for degradation to inhibit type III interferon expression in intestinal
625 epithelial cells', *Elife,* 7.
626 Dittmar, M., Lee, J. S., Whig, K., Segrist, E., Li, M., Kamalia, B., Castellana, L., Ayyanathan, K., Truitt,
627 R., Yang, W., Jurado, K., Samby, K., Ramage, H., Schultz, D. and Cherry, S. (2021) 'Drug repurposing
628 screens reveal cell-type specific entry pathways and FDA approved drugs active against SARS-
629 Cov-2', *Cell Rep*.
630 Gao, Y., Yan, L., Huang, Y., Liu, F., Zhao, Y., Cao, L., Wang, T., Sun, Q., Ming, Z., Zhang, L., Ge, J.,
631 Zheng, L., Zhang, Y., Wang, H., Zhu, Y., Zhu, C., Hu, T., Hua, T., Zhang, B., Yang, X., Li, J., Yang, H.,

632 Liu, Z., Xu, W., Guddat, L. W., Wang, Q., Lou, Z. and Rao, Z. (2020) 'Structure of the RNA-
633 dependent RNA polymerase from COVID-19 virus', *Science,* 368(6492), pp. 779-782.
634 Guo, R., Fan, B., Chang, X., Zhou, J., Zhao, Y., Shi, D., Yu, Z., He, K. and Li, B. (2020)
635 'Characterization and evaluation of the pathogenicity of a natural recombinant transmissible
636 gastroenteritis virus in China', *Virology,* 545, pp. 24-32.
637 Heiser, K., McLean, P. F., Davis, C. T., Fogelson, B., Gordon, H. B., Jacobson, P., Hurst, B., Miller,
638 B., Alfa, R. W., Earnshaw, B. A., Victors, M. L., Chong, Y. T., Haque, I. S., Low, A. S. and Gibson, C.
639 C. (2020) 'Identification of potential treatments for COVID-19 through artificial intelligence-
640 enabled phenomic analysis of human cells infected with SARS-CoV-2', *bioRxiv*.
641 Hemeryck, A. and Belpaire, F. M. (2002) 'Selective serotonin reuptake inhibitors and cytochrome
642 P-450 mediated drug-drug interactions: an update', *Curr Drug Metab,* 3(1), pp. 13-37.
643 Hoffmann, M., Kleine-Weber, H., Schroeder, S., Kruger, N., Herrler, T., Erichsen, S., Schiergens, T.
644 S., Herrler, G., Wu, N. H., Nitsche, A., Muller, M. A., Drosten, C. and Pohlmann, S. (2020) 'SARS-
645 CoV-2 Cell Entry Depends on ACE2 and TMPRSS2 and Is Blocked by a Clinically Proven Protease
646 Inhibitor', *Cell*.
647 Hou, Y. J., Okuda, K., Edwards, C. E., Martinez, D. R., Asakura, T., Dinnon, K. H., 3rd, Kato, T., Lee,
648 R. E., Yount, B. L., Mascenik, T. M., Chen, G., Olivier, K. N., Ghio, A., Tse, L. V., Leist, S. R., Gralinski,
649 L. E., Schafer, A., Dang, H., Gilmore, R., Nakano, S., Sun, L., Fulcher, M. L., Livraghi-Butrico, A.,
650 Nicely, N. I., Cameron, M., Cameron, C., Kelvin, D. J., de Silva, A., Margolis, D. M., Markmann, A.,
651 Bartelt, L., Zumwalt, R., Martinez, F. J., Salvatore, S. P., Borczuk, A., Tata, P. R., Sontake, V., Kimple,
652 A., Jaspers, I., O'Neal, W. K., Randell, S. H., Boucher, R. C. and Baric, R. S. (2020) 'SARS-CoV-2
653 Reverse Genetics Reveals a Variable Infection Gradient in the Respiratory Tract', *Cell*.
654 Ianevski, A., He, L., Aittokallio, T. and Tang, J. (2020) 'SynergyFinder: a web application for
655 analyzing drug combination dose-response matrix data', *Bioinformatics,* 36(8), pp. 2645.
656 Jin, Z., Du, X., Xu, Y., Deng, Y., Liu, M., Zhao, Y., Zhang, B., Li, X., Zhang, L., Peng, C., Duan, Y., Yu,
657 J., Wang, L., Yang, K., Liu, F., Jiang, R., Yang, X., You, T., Liu, X., Yang, X., Bai, F., Liu, H., Liu, X.,
658 Guddat, L. W., Xu, W., Xiao, G., Qin, C., Shi, Z., Jiang, H., Rao, Z. and Yang, H. (2020) 'Structure of
659 M(pro) from SARS-CoV-2 and discovery of its inhibitors', *Nature,* 582(7811), pp. 289-293.
660 Kang, Y. L., Chou, Y. Y., Rothlauf, P. W., Liu, Z., Soh, T. K., Cureton, D., Case, J. B., Chen, R. E.,
661 Diamond, M. S., Whelan, S. P. J. and Kirchhausen, T. (2020) 'Inhibition of PIKfyve kinase prevents
662 infection by Zaire ebolavirus and SARS-CoV-2', *Proc Natl Acad Sci U S A,* 117(34), pp. 20803-20813.
663 Karchner, S. I., Franks, D. G., Powell, W. H. and Hahn, M. E. (2002) 'Regulatory interactions among
664 three members of the vertebrate aryl hydrocarbon receptor family: AHR repressor, AHR1, and
665 AHR2', *J Biol Chem,* 277(9), pp. 6949-59.
666 Kim, M. S., Cho, H. I., Yoon, H. J., Ahn, Y. H., Park, E. J., Jin, Y. H. and Jang, Y. K. (2018) 'JIB-04, A
667 Small Molecule Histone Demethylase Inhibitor, Selectively Targets Colorectal Cancer Stem Cells
668 by Inhibiting the Wnt/beta-Catenin Signaling Pathway', *Sci Rep,* 8(1), pp. 6611.
669 Kirchdoerfer, R. N. and Ward, A. B. (2019) 'Structure of the SARS-CoV nsp12 polymerase bound
670 to nsp7 and nsp8 co-factors', *Nat Commun,* 10(1), pp. 2342.
671 Li, B., Ding, S., Feng, N., Mooney, N., Ooi, Y. S., Ren, L., Diep, J., Kelly, M. R., Yasukawa, L. L., Patton,
672 J. T., Yamazaki, H., Shirao, T., Jackson, P. K. and Greenberg, H. B. (2017) 'Drebrin restricts rotavirus
673 entry by inhibiting dynamin-mediated endocytosis', *Proc Natl Acad Sci U S A,* 114(18), pp. E3642-
674 E3651.

675 Luo, L., Wang, S., Zhu, L., Fan, B., Liu, T., Wang, L., Zhao, P., Dang, Y., Sun, P., Chen, J., Zhang, Y.,
676 Chang, X., Yu, Z., Wang, H., Guo, R., Li, B. and Zhang, K. (2019) 'Aminopeptidase N-null neonatal
677 piglets are protected from transmissible gastroenteritis virus but not porcine epidemic diarrhea
678 virus', *Sci Rep,* 9(1), pp. 13186.
679 Mirabelli, C., Wotring, J. W., Zhang, C. J., McCarty, S. M., Fursmidt, R., Frum, T., Kadambi, N. S.,
680 Amin, A. T., O'Meara, T. R., Pretto, C. D., Spence, J. R., Huang, J., Alysandratos, K. D., Kotton, D.
681 N., Handelman, S. K., Wobus, C. E., Weatherwax, K. J., Mashour, G. A., O'Meara, M. J. and Sexton,
682 J. Z. (2020) 'Morphological Cell Profiling of SARS-CoV-2 Infection Identifies Drug Repurposing
683 Candidates for COVID-19', *bioRxiv*.
684 Nguyen, H. L., Thai, N. Q., Truong, D. T. and Li, M. S. (2020) 'Remdesivir Strongly Binds to Both
685 RNA-Dependent RNA Polymerase and Main Protease of SARS-CoV-2: Evidence from Molecular
686 Simulations', *J Phys Chem B,* 124(50), pp. 11337-11348.
687 Ou, X., Liu, Y., Lei, X., Li, P., Mi, D., Ren, L., Guo, L., Guo, R., Chen, T., Hu, J., Xiang, Z., Mu, Z., Chen,
688 X., Chen, J., Hu, K., Jin, Q., Wang, J. and Qian, Z. (2020) 'Characterization of spike glycoprotein of
689 SARS-CoV-2 on virus entry and its immune cross-reactivity with SARS-CoV', *Nat Commun,* 11(1),
690 pp. 1620.
691 Parrish, J. K., McCann, T. S., Sechler, M., Sobral, L. M., Ren, W., Jones, K. L., Tan, A. C. and Jedlicka,
692 P. (2018) 'The Jumonji-domain histone demethylase inhibitor JIB-04 deregulates oncogenic
693 programs and increases DNA damage in Ewing Sarcoma, resulting in impaired cell proliferation
694 and survival, and reduced tumor growth', *Oncotarget,* 9(69), pp. 33110-33123.
695 Riva, L., Yuan, S., Yin, X., Martin-Sancho, L., Matsunaga, N., Pache, L., Burgstaller-Muehlbacher,
696 S., De Jesus, P. D., Teriete, P., Hull, M. V., Chang, M. W., Chan, J. F., Cao, J., Poon, V. K., Herbert,
697 K. M., Cheng, K., Nguyen, T. H., Rubanov, A., Pu, Y., Nguyen, C., Choi, A., Rathnasinghe, R.,
698 Schotsaert, M., Miorin, L., Dejosez, M., Zwaka, T. P., Sit, K. Y., Martinez-Sobrido, L., Liu, W. C.,
699 White, K. M., Chapman, M. E., Lendy, E. K., Glynne, R. J., Albrecht, R., Ruppin, E., Mesecar, A. D.,
700 Johnson, J. R., Benner, C., Sun, R., Schultz, P. G., Su, A. I., Garcia-Sastre, A., Chatterjee, A. K., Yuen,
701 K. Y. and Chanda, S. K. (2020) 'Discovery of SARS-CoV-2 antiviral drugs through large-scale
702 compound repurposing', *Nature,* 586(7827), pp. 113-119.
703 Saif, L. J. (2004) 'Animal coronavirus vaccines: lessons for SARS', *Dev Biol (Basel),* 119, pp. 129-40.
704 Schneider, W. M., Luna, J. M., Hoffmann, H. H., Sanchez-Rivera, F. J., Leal, A. A., Ashbrook, A. W.,
705 Le Pen, J., Ricardo-Lax, I., Michailidis, E., Peace, A., Stenzel, A. F., Lowe, S. W., MacDonald, M. R.,
706 Rice, C. M. and Poirier, J. T. (2021) 'Genome-Scale Identification of SARS-CoV-2 and Pan-
707 coronavirus Host Factor Networks', *Cell,* 184(1), pp. 120-132 e14.
708 Sheahan, T. P., Sims, A. C., Zhou, S., Graham, R. L., Pruijssers, A. J., Agostini, M. L., Leist, S. R.,
709 Schafer, A., Dinnon, K. H., 3rd, Stevens, L. J., Chappell, J. D., Lu, X., Hughes, T. M., George, A. S.,
710 Hill, C. S., Montgomery, S. A., Brown, A. J., Bluemling, G. R., Natchus, M. G., Saindane, M.,
711 Kolykhalov, A. A., Painter, G., Harcourt, J., Tamin, A., Thornburg, N. J., Swanstrom, R., Denison,
712 M. R. and Baric, R. S. (2020) 'An orally bioavailable broad-spectrum antiviral inhibits SARS-CoV-2
713 in human airway epithelial cell cultures and multiple coronaviruses in mice', *Sci Transl Med,*
714 12(541).
715 Touret, F., Gilles, M., Barral, K., Nougairede, A., van Helden, J., Decroly, E., de Lamballerie, X. and
716 Coutard, B. (2020) 'In vitro screening of a FDA approved chemical library reveals potential
717 inhibitors of SARS-CoV-2 replication', *Sci Rep,* 10(1), pp. 13093.

718 Wang, L., Chang, J., Varghese, D., Dellinger, M., Kumar, S., Best, A. M., Ruiz, J., Bruick, R., Pena-
719 Llopis, S., Xu, J., Babinski, D. J., Frantz, D. E., Brekken, R. A., Quinn, A. M., Simeonov, A., Easmon,
720 J. and Martinez, E. D. (2013) 'A small molecule modulates Jumonji histone demethylase activity
721 and selectively inhibits cancer growth', *Nat Commun,* 4, pp. 2035.
722 Wang, M., Cao, R., Zhang, L., Yang, X., Liu, J., Xu, M., Shi, Z., Hu, Z., Zhong, W. and Xiao, G. (2020a)
723 'Remdesivir and chloroquine effectively inhibit the recently emerged novel coronavirus (2019-
724 nCoV) in vitro', *Cell Res,* 30(3), pp. 269-271.
725 Wang, R., Simoneau, C. R., Kulsuptrakul, J., Bouhaddou, M., Travisano, K. A., Hayashi, J. M.,
726 Carlson-Stevermer, J., Zengel, J. R., Richards, C. M., Fozouni, P., Oki, J., Rodriguez, L., Joehnk, B.,
727 Walcott, K., Holden, K., Sil, A., Carette, J. E., Krogan, N. J., Ott, M. and Puschnik, A. S. (2021)
728 'Genetic Screens Identify Host Factors for SARS-CoV-2 and Common Cold Coronaviruses', *Cell,*
729 184(1), pp. 106-119 e14.
730 Wang, X., Cao, R., Zhang, H., Liu, J., Xu, M., Hu, H., Li, Y., Zhao, L., Li, W., Sun, X., Yang, X., Shi, Z.,
731 Deng, F., Hu, Z., Zhong, W. and Wang, M. (2020b) 'The anti-influenza virus drug, arbidol is an
732 efficient inhibitor of SARS-CoV-2 in vitro', *Cell Discov,* 6, pp. 28.
733 Wei, J., Alfajaro, M. M., DeWeirdt, P. C., Hanna, R. E., Lu-Culligan, W. J., Cai, W. L., Strine, M. S.,
734 Zhang, S. M., Graziano, V. R., Schmitz, C. O., Chen, J. S., Mankowski, M. C., Filler, R. B., Ravindra,
735 N. G., Gasque, V., de Miguel, F. J., Patil, A., Chen, H., Oguntuyo, K. Y., Abriola, L., Surovtseva, Y.
736 V., Orchard, R. C., Lee, B., Lindenbach, B. D., Politi, K., van Dijk, D., Kadoch, C., Simon, M. D., Yan,
737 Q., Doench, J. G. and Wilen, C. B. (2021) 'Genome-wide CRISPR Screens Reveal Host Factors
738 Critical for SARS-CoV-2 Infection', *Cell,* 184(1), pp. 76-91 e13.
739 Wu, F., Zhao, S., Yu, B., Chen, Y. M., Wang, W., Song, Z. G., Hu, Y., Tao, Z. W., Tian, J. H., Pei, Y. Y.,
740 Yuan, M. L., Zhang, Y. L., Dai, F. H., Liu, Y., Wang, Q. M., Zheng, J. J., Xu, L., Holmes, E. C. and Zhang,
741 Y. Z. (2020) 'A new coronavirus associated with human respiratory disease in China', *Nature,*
742 579(7798), pp. 265-269.
743 Xie, X., Muruato, A., Lokugamage, K. G., Narayanan, K., Zhang, X., Zou, J., Liu, J., Schindewolf, C.,
744 Bopp, N. E., Aguilar, P. V., Plante, K. S., Weaver, S. C., Makino, S., LeDuc, J. W., Menachery, V. D.
745 and Shi, P. Y. (2020) 'An Infectious cDNA Clone of SARS-CoV-2', *Cell Host Microbe*.
746 Xu, M., Moresco, J. J., Chang, M., Mukim, A., Smith, D., Diedrich, J. K., Yates, J. R., 3rd and Jones,
747 K. A. (2018) 'SHMT2 and the BRCC36/BRISC deubiquitinase regulate HIV-1 Tat K63-ubiquitylation
748 and destruction by autophagy', *PLoS Pathog,* 14(5), pp. e1007071.
749 Yin, W., Mao, C., Luan, X., Shen, D. D., Shen, Q., Su, H., Wang, X., Zhou, F., Zhao, W., Gao, M.,
750 Chang, S., Xie, Y. C., Tian, G., Jiang, H. W., Tao, S. C., Shen, J., Jiang, Y., Jiang, H., Xu, Y., Zhang, S.,
751 Zhang, Y. and Xu, H. E. (2020) 'Structural basis for inhibition of the RNA-dependent RNA
752 polymerase from SARS-CoV-2 by remdesivir', *Science*.
753 Zang, R., Case, J. B., Yutuc, E., Ma, X., Shen, S., Gomez Castro, M. F., Liu, Z., Zeng, Q., Zhao, H.,
754 Son, J., Rothlauf, P. W., Kreutzberger, A. J. B., Hou, G., Zhang, H., Bose, S., Wang, X., Vahey, M. D.,
755 Mani, K., Griffiths, W. J., Kirchhausen, T., Fremont, D. H., Guo, H., Diwan, A., Wang, Y., Diamond,
756 M. S., Whelan, S. P. J. and Ding, S. (2020a) 'Cholesterol 25-hydroxylase suppresses SARS-CoV-2
757 replication by blocking membrane fusion', *Proc Natl Acad Sci U S A,* 117(50), pp. 32105-32113.
758 Zang, R., Gomez Castro, M. F., McCune, B. T., Zeng, Q., Rothlauf, P. W., Sonnek, N. M., Liu, Z.,
759 Brulois, K. F., Wang, X., Greenberg, H. B., Diamond, M. S., Ciorba, M. A., Whelan, S. P. J. and Ding,
760 S. (2020b) 'TMPRSS2 and TMPRSS4 promote SARS-CoV-2 infection of human small intestinal
761 enterocytes', *Sci Immunol,* 5(47).

762 Zhang, L., Lin, D., Sun, X., Curth, U., Drosten, C., Sauerhering, L., Becker, S., Rox, K. and Hilgenfeld,
763 R. (2020) 'Crystal structure of SARS-CoV-2 main protease provides a basis for design of improved
764 alpha-ketoamide inhibitors', *Science,* 368(6489), pp. 409-412.
765 Zhou, P., Yang, X. L., Wang, X. G., Hu, B., Zhang, L., Zhang, W., Si, H. R., Zhu, Y., Li, B., Huang, C. L.,
766 Chen, H. D., Chen, J., Luo, Y., Guo, H., Jiang, R. D., Liu, M. Q., Chen, Y., Shen, X. R., Wang, X., Zheng,
767 X. S., Zhao, K., Chen, Q. J., Deng, F., Liu, L. L., Yan, B., Zhan, F. X., Wang, Y. Y., Xiao, G. F. and Shi,
768 Z. L. (2020) 'A pneumonia outbreak associated with a new coronavirus of probable bat origin',
769 *Nature,* 579(7798), pp. 270-273.
770
771

772 **Funding**

773

774 This study is supported by the National Institutes of Health (NIH) DDRCC grant P30
775 DK052574, NIH grants K99/R00 AI135031 and R01 AI150796 and the COVID-19 Fast
776 Grants Funding to S.D., NIH contracts and grants (75N93019C00062 and R01 AI127828)
777 and the Defense Advanced Research Project Agency (HR001117S0019) to M.S.D., NIH
778 grant U01 AI151810 to A.C.M.B., and unrestricted funds from Washington University
779 School of Medicine and NIH grant R37 AI059371 to S.P.W. This study is partly funded by
780 The Welch Foundation grant (I-1878) and NIH grant (R21AI139408) to E.D.M. The *in vivo*
781 pig studies are supported by the Jiangsu Province Natural Sciences Foundation
782 (BK20190003) and National Natural Science Foundation of China (31872481) to B.L.
783 J.B.C. is supported by a Helen Hay Whitney Foundation postdoctoral fellowship.

784

785 **Author contributions**

786

787 J.S., Q.Z., R.Z., and S.D. designed, executed, and analyzed *in vitro* efficacy studies.
788 M.F.G.C., H.P.K., and G.H. assisted with the RNA extraction and RT-qPCR analysis. Y.Z.
789 performed the *in vitro* TGEV inhibition studies. Z.L. performed the flow cytometry analysis.
790 L.C. wrote the algorithm that quantifies inhibitor screen results. P.W.R. and S.P.J.W.
791 constructed the VSV-SARS-CoV-2 virus. E.D.M. provided JIB-04 Z-isomer. Q.Z., J.Z.,
792 and R.G. propagated and titrated viruses. J.B.C. propagated and infected the clinical
793 isolate of SARS-CoV-2. P.Y.S. provided the recombinant SARS-CoV-2 mNeonGreen
794 virus. A.L.B propagated the mNeonGreen virus and designed the SARS-CoV-2 Taqman

probe. S.H., B.L., and S.D. designed the *in vivo* efficacy studies. S.H., J.Z., X.C., B.F., and B.N., performed the *in vivo* TGEV infection experiments, dissected the animals and harvested tissues, and measured viral titers and cytokine mRNA levels. X.W., E.D.M., S.P.J.W., M.S.D., A.C.M.B., B.L., and S.D. provided supervision and funding for the study. J.S. and S.D. wrote the manuscript with the input and edits from S.H., Q.Z., J.B.C., J.Z., Z.L., M.F.G.C., H.P.K., G.H., S.P.J.W., M.S.D., A.C.M.B., and B.L.

Competing interests

The Boon laboratory has scientific research agreements with AI therapeutics, Greenlight Biosciences and Nano Targeting & Therapy Biopharma Inc. M.S.D. is a consultant for Inbios, Eli Lilly, Vir Biotechnology, NGM Biopharmaceuticals, and Emergent BioSolutions and on the Scientific Advisory Boards of Moderna and Immunome. The Diamond laboratory at Washington University School of Medicine has received unrelated sponsored research agreements from Moderna, Vir Biotechnology, and Emergent BioSolutions.

Acknowledgements

The authors thank Dr. Harry Greenberg (Stanford University, USA) and Dr. Bolívar A. Villacís-Bermeo (Guayaquil, Guayas, Ecuador) for constructive comments and arguments. We appreciate the assistance from Matthew Williams (Department of Molecular Microbiology Media and Glassware Facility) and Erica Lantelme (Department

818 of Pathology and Immunology, Flow Cytometry Core Facility). Cytation plate scanning
819 was assisted by Zhou Huang (Department of Molecular Microbiology).
820

821 **Data and materials availability**

822

823 All raw data in the current study are available in Table S3 and Dataset S1. RNA-seq
824 dataset has been deposited onto NCBI GEO (GSE156219).

825